

An Advanced Two-Stage Grid Connected PV System: A Fractional-Order Controller

Shah Fahad*, Nasim Ullah**, Ali Jafer Mahdi***, Asier Ibeas****, Arman Goudarzi*‡

* College of Electrical Engineering, Zhejiang University, Hangzhou, China

**Department of Electrical Engineering, University of Technology, Nowshera, Pakistan

***Department of Electrical and Electronics Engineering, University of Kerbala, Iraq

****Escola d'Enginyeria, Universitat Autònoma de Barcelona, Barcelona, Spain

(shah.fahad072@zju.edu.cn , nasim.ullah@uotnowshera.edu.pk, ali.j.mahdi@uokerbala.edu.iq, asier.ibeas@uab.cat, agoudarzi@zju.edu.cn)

‡

Corresponding Author; Last Author, College of Electrical, Zhejiang University, Hangzhou, China

Tel: +86 137 7789 4042, agoudarzi@zju.edu.cn

Received: 16.01.2019 Accepted: 27.02.2019

Abstract- A fractional-order (FO) based controller for a grid-connected PV system is presented in this paper. A single phase two-stage grid-connected photovoltaic generator (PVG) is used to test the performance of the FO controller. The main objectives of the proposed controller are: (1) To regulate the output voltage of PVG at a point where the maximum power is drawn. (2) Constant DC-link voltage control. (3) Power factor control (PFC) at the inverter output with low total harmonic distortion (THD). To solve the first problem, a non-linear control method known as fractional-order back-stepping control (FOBSC) is used to regulate the output voltage of PVG. A maximum power point tracking (MPPT) technique known as perturb and observe (P&O) is used to generate a reference voltage which is suitable for tracking the maximum power generation of PVG. The generated reference is used to regulate the output voltage of PVG using FOBSC. The DC-link voltage fluctuation issue is tackled using FO based PI controller. The last objective is achieved using FOBSC to obtain maximum power factor of the grid. Lyapunov candidate function is used to verify the stability of the system. To test the performance of the proposed controller, it is compared to conventionally known Integer-order (IO) controller. Results have shown a significant improvement in THD and efficiency of the system. The proposed controller offers 0.94%, 1.43% and 1.86% lower THD in comparison with IO controller at 100%, 80% and 70% of the power generation capacity of PVG, respectively. The overall efficiency of the system for 100%, 80%, and 70% of the dynamic powers of the system is noticed to be better in case of FO controller.

Keywords Photovoltaic generator (PVG); fractional-order (FO), integer-order (IO), back-stepping control (BSC).

Nomenclature

Indexes

BSC	Back-stepping controller
FO	Fractional-order
FOBSC	Fractional-order back-stepping control
FOPI	Fractional-order proportional integral
IO	Integral-order
IOBS	Integral-order back-stepping
IV-Curve	Current-voltage curve of a photovoltaic generator

MPPT

Maximum power point tracking

P & O

Perturb and observe

PVG

Photovoltaic generator

PF

Power factor

RCC

Ripple co-relation control

THD

Total harmonic distortion

Variables

${}_a D_t^\alpha$	Fractional-order operator
α	Fractional-order operator's coefficient
C_{dc}	DC-link capacitor
C_{pv}	Capacitor parallel to PVG
I_o	Boost converter inductor current
K_I	Integral constant of PI controller
K_P	Proportional constant of PI controller
L_g	Grid inductor
L_o	Boost converter inductor
M_1, M_2	Alternate switches (1 and 2) of inverter
M_3, M_4	Alternate switches (3 and 4) of inverter
V_{dc}	Voltage across DC-link capacitor
V_g	Grid voltage
V_1, V_2	Lyapunov stability candidate functions
α_1	FOBSC tuning order 1
α_2	FOBSC tuning order 2

1. Introduction

In the past few decades, because of the rapid increase in population and global industrialization, demand for electricity has grown substantially. Due to abundance of renewable resources in nature, solar energy is considered as one of the most promising forms of renewable energy resources. Solar energy has zero fuel cost and also it is an environmentally friendly source of energy. Much interest is being taken in designing an efficient PV system in which it has fewer grid-connectivity challenges such as grid stability, generation intermittency, power mismatch and etc. have been investigated [1, 2, 4, 38, 39].

Generally, PVGs have two major flaws. The first and most important one is the efficiency which has been calculated as low as 9-16% according to [6]. The other drawback is non-linearity of current-voltage (IV) characteristic of PV generation unit. The IV-characteristic of PVG changes with irradiance and the ambient temperature of the cells [7].

Non-linearity of the PVG unit has been one of the major concerns of researchers while studying the integration of solar energy. To tackle this problem, a technique called maximum power point tracking (MPPT) is used to extract maximum power from the PV source and deliver it to the load [5]. In this study, the P&O method is used for the implementation of MPPT and enhancing the converter efficiency. The efficiency of the implemented P&O

algorithm is about 91.4% at the full irradiance condition and 95.6% at the partial cloudy conditions [5, 9].

For the operation of a PV system, a DC-DC converter is required to increase the output voltage of the PVG unit higher than the grid nominal voltage to ensure the uni-directional power flow from source to the grid. In this regard, for a grid-tied inverter configuration, a DC-DC boost converter is required to provide a constant power flow to the input of inverter [8, 10].

The power balance is essential to be maintained on the DC-link side. At the time that the power is being fed to the inverter through the DC-link, the voltage of the DC-link varies with power transfer. As the power flow-towards the DC-link increases, accordingly the voltage across it increases [10, 11, 40]. Thus, the input to the inverter changes with a change in voltage of DC-link. Therefore, a feedback control loop is required to keep the voltage across DC-link constant.

With respect to the above-mentioned reasons, an important consideration for a grid-connected PV inverter is to regulate the DC-link voltage to a level higher than grid voltage. Therefore, it is necessary to insert a filter before feeding the power to the grid in order to reduce the THD produced due to the high switching frequency of the PV inverter. As per IEEE standards, the total permissible THD of a grid-tied inverter should be less than 5% [3].

In [30], the authors claim to have presented a cost-effective grid-connected PV inverter. The THD at full load is achieved at 6.7% using an LC filter which is still above the IEEE THD grid code standard. The author in [22], has applied a hybrid technique for optimizing switching angles of the inverter for eliminating selective harmonics. A lot of work has been done in finding the appropriate mathematical solutions while the THD is reduced only to 4.61%. In [25], a control method based on virtual impedance for increasing output impedance of inverter is used to improve the system stability, where the THD could be reduced to 4.12%. In [32], a simplified DQ controller for a PV system has been presented. Although the chance of ripple attenuation using LCL filter is higher, the obtained THD was not noticeably low.

Active and reactive power control strategy has been implemented for grid-connected PV inverter by the authors in [24], in which the control system is based on dq-transformation. In [23], ripple co-relation control (RCC) is discussed which has a drawback of unstable behaviour during irradiance variation. An improved control method called hybrid RCC is proposed which mitigates the drawback of previous control. In [12], [21-26] and [33-35], the authors proposed integer order back-stepping control and integer order integral back-stepping control respectively. In [7], the author has applied a variable structure control for tuning power factor along with DC-link voltage control and maximum power point tracking. In [31], the study presented an adaptive filtering method for reducing THD by addressing double line frequency voltage ripples in voltage across dc-link. In this study, the THD has been reduced, whereas a quantitative analysis was not presented. In all the aforementioned papers, the studies were based on power

quality but lack quantitative analysis. To the best of our knowledge, the fractional order back-stepping controller for a two-stage grid-connected PV inverter using L filter has never been considered. The slow and intense decay nature of fractional order derivative and integral can be further exploited to achieve a better power quality in a grid-connected PV system. A fractional order controller allows more degree of freedom as compared to an integer order controller. A simple L filter is preferred over LC and LCL filter for PV systems due to the following features: (i) simplicity in design, (ii) low cost and (iii) lack of resonant effect [29]. Furthermore, the stability proof using Lyapunov stability theory is presented. A simple L-filter has only one dynamic equation to be considered for the stability proof in Lyapunov stability theory, thereby, leads to reduction of complexity in deriving the essential equations.

In this article, the power quality enhancement has been given a priority. Reducing the THD and increasing the efficiency of the system by exploiting the slow and intense nature of the FO controller is the main contribution of this work. FO controller has a wider range of stability margins as well as the release of energy is less and slower as compared to the integer order system. Based on the previously discussed literature, fractional order back-stepping controller for PV inverters has never been discussed. This article proposes the implementation and derivation of fractional order back-stepping controller (FOBSC) for tracking the reference voltage generated by the MPPT and power factor

control for sine wave grid-connected PV inverter. The P&O algorithm is used to generate a voltage reference which is traced by FOBS controller. The DC-link voltage is regulated using a fractional order PI (FOPI) controller. Finally, the current through L-filter is regulated to the phase of grid voltage using FOBSC to achieve unity power factor.

The main contributions of the study can be listed as follows:

- A fractional order back-stepping controller (FOBSC) is derived and implemented for a two-stage grid-connected PV inverter which uses an L-filter to enhance THD.
- The slow and intense nature of fractional order controller has been exploited to enhance the power quality of the PV system.
- A comparison between the proposed fractional order back-stepping controller (FOBSC) to a conventional integer order controller is presented in terms of power quality.

This paper is presented in the following manner: In section 2 mathematical model of the complete system is given. Derivation of the proposed controller is presented in section 3. Simulation results and discussions are given in section 4. Section 5 summarizes the conclusions of all the work that has presented in this research.

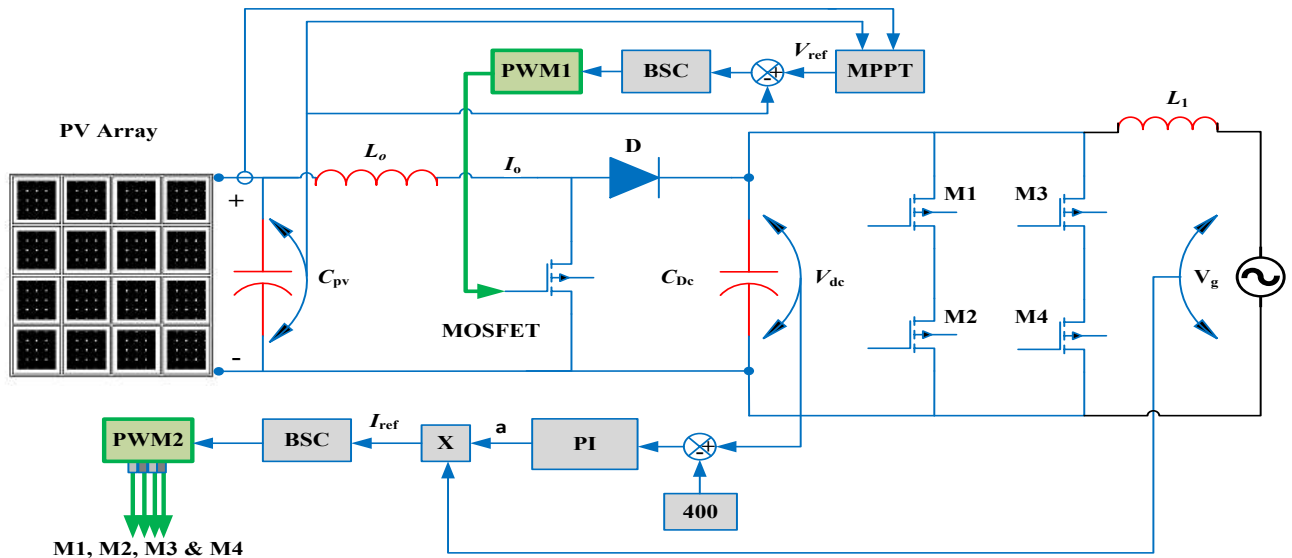


Fig. 1: Block diagram of the complete system

2. Mathematical Preliminaries and Modelling

The complete circuit diagram along with the controller layout is given in Fig. 1. The DC-link capacitor, denoted by C_{DC} , plays an important role of feeding a constant DC power to the inverter. For better understanding of the proposed idea, the system can be divided into two parts. From the left-hand side to the DC-link capacitor is the DC part which includes

PVG and the boost converter. The second part of the system, is the

AC part in which a constant DC-link voltage is fed to an inverter to convert it to AC power. This inverted power consists of harmonic distortions due to high switching frequency mechanism of the inverter, therefore a filter is used to reduce THD and feed this power to the grid.

2.1 Photovoltaic Module

The PVG used in this system has an IV-Characteristic curve shown in Fig. 7a and 7b.

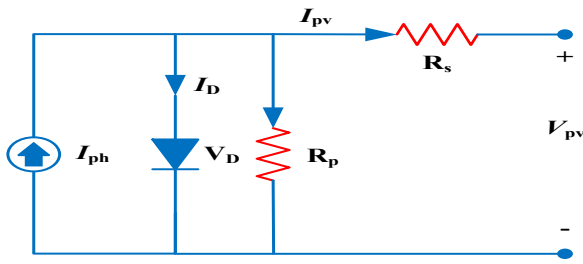


Fig. 2: Electrical Representation of PVG

The current generated by a PV module is presented in the following equation:

$$I_{pv} = I_{ph} - I_o \left[\exp\left(\frac{q(V+IR_s)}{N_s K T A}\right) - 1 \right] - (V + IR_s)/(R_p) \quad (1)$$

Where q is electron charge, K is the Boltzmann Constant, T is the PV module temperature, I_o is the reverse saturation current of the diode, A is the diode ideality constant, I_{ph} is the light generated current of PV cell, R_p is the shunt resistance of PV cell, R_s is the series resistance of the PV cell, N_s is the number of the PV module connected in series and I_{pv} is the output current [28].

2.2 DC-DC Boost Converter

A DC-DC boost converter provides an interface between PVG and inverter while allowing us to implement different control strategies including MPPT. A PV inverter requires a constant DC input voltage to operate at its best. A stable input voltage with least ripples can promise a better inverter output [37, 41]. Hence, a boost converter as shown in Fig. 3 is attached between inverter and PVG to keep the input voltage to the inverter constant. A boost converter consists of an inductor, dc-link capacitor (output capacitor), a transistor and a diode [42].

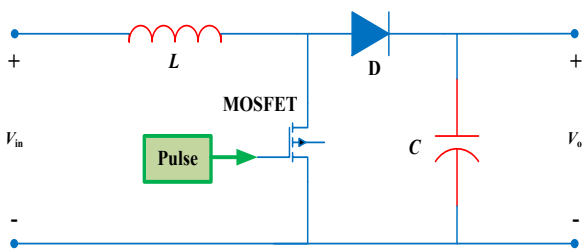


Fig. 3: Boost Converter

$$L_{min} \geq \frac{V_{in}(V_{out}-V_{in})}{\Delta I * V_{out} * f_s} \quad (2)$$

$$V_{out} = \frac{V_i}{1-D} \quad (3)$$

$$D = \frac{t_{on}}{T} \quad (4)$$

Where D is the duty cycle, t_{on} is the time for which switch is turned on, f_s is the switching frequency of the boost converter, L_{min} is the minimum input inductance of the boost converter. The output of the PV inverter capacitor of the boost converter is measured through the following equation:

$$C_{dc} = \frac{P_g}{\Delta V V_{dc} \omega} \quad (5)$$

Where P_g is the power generated by PVG, ΔV is the voltage ripple normally kept about 10% of total voltage, V_{dc} is the DC-link voltage, ω is the grid angular frequency. Any further required explanation for the classical inverter has been given in [36].

2.3 Mathematical Background of the Fractional-Order Operator

In this section, the mathematical preliminaries are introduced for the non-integer order calculus. Fractional-order operator is defined as ${}_a D_t^\alpha$

$${}_a D_t^\alpha \cong D^\alpha = \begin{cases} \frac{d^\alpha}{dt^\alpha} & , R(\alpha) > 0 \\ 1 & , R(\alpha) = 0 \\ \int_a^t (d\tau)^{-\alpha} & , R(\alpha) < 0 \end{cases} \quad (6)$$

In the above equation, α represents fractional operator's order, while $R(\alpha)$ represents the set of real numbers. Three main definitions of general fractional operators are discussed below [16]:

Definition 1: The α^{th} order Riemann–Liouville fractional derivative and integration of a function $f(t)$ with respect to t is given by:

$${}_a D_t^\alpha f(t) = \frac{d^\alpha}{dt^\alpha} f(t) = \frac{1}{\Gamma(m-\alpha)} \frac{d^m}{dt^m} \int_a^t \frac{f(\tau)}{(t-\tau)^{\alpha-m+1}} d\tau \quad (7)$$

$${}_a D_t^{-\alpha} f(t) = I^\alpha f(t) = \frac{1}{\Gamma(\alpha)} \int_a^t \frac{f(\tau)}{(t-\tau)^{1-\alpha}} d\tau \quad (8)$$

In the aforementioned equation, the term 'm' is the first integer larger than "a", such as $m - 1 < \alpha < m$, and $t - \alpha$ is the interval of integration and $\Gamma(\alpha)$ is Euler's Gamma function.

Definition 2: The α^{th} order Caputo fractional derivative expression of a continuous function is formulated as follows:

$${}_a D_t^\alpha \cong D^\alpha = \begin{cases} \frac{1}{\Gamma(n-\alpha)} \int_a^t \frac{f^n(\tau)}{(t-\tau)^{\alpha-n+1}} d\tau & (n - 1 \leq \alpha < n) \\ \frac{d^n}{dt^n} f(t) & (\alpha = n) \end{cases} \quad (9)$$

Definition 3: The GL definition of order α is stated as follows:

$${}^G L D_t^\alpha f(t) = \lim_{h \rightarrow 0} \frac{1}{h^\alpha} \sum_{j=0}^{[(t-\alpha)/h]} (-1)^j \binom{\alpha}{j} f(t-jh) \tag{10}$$

$$\binom{\alpha}{j} = \frac{\Gamma(\alpha+1)}{\Gamma(j+1)\Gamma(\alpha-j+1)} \tag{11}$$

In the above equation, the term ‘h’ represents the time step and $\Gamma(\cdot)$ represents the gamma function. In [15, 17], the stability of fractional order systems has been discussed in details. To approximate the fractional orders by classical integer order transfer function, an oustaloup recursive approximation algorithm is used. In [18], an oustaloup recursive approximation algorithm is discussed in detail.

2.4 Fractional Order Dynamics and Total Harmonic Distortion

Advantages of FO controllers have been presented in [19-21]. This section is dedicated to compare the energy decay property of the integer order with fractional order systems in the fractional range of $0 < \alpha < 1$.

From Fig. 4, it is evident that the release of energy in the case of fractional order systems is less and slower as compared to the integer order systems.

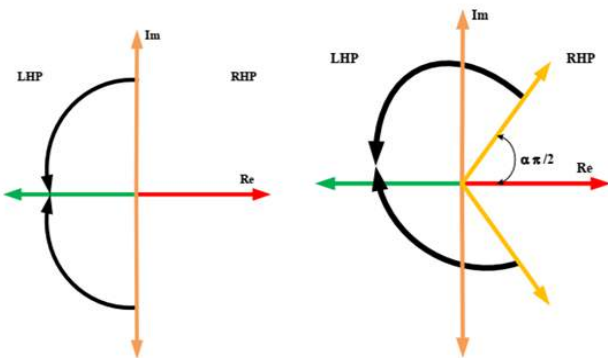


Fig. 4: Stability Region of:(a) Integer Order controller on the left. (b) Fractional Order on the right.

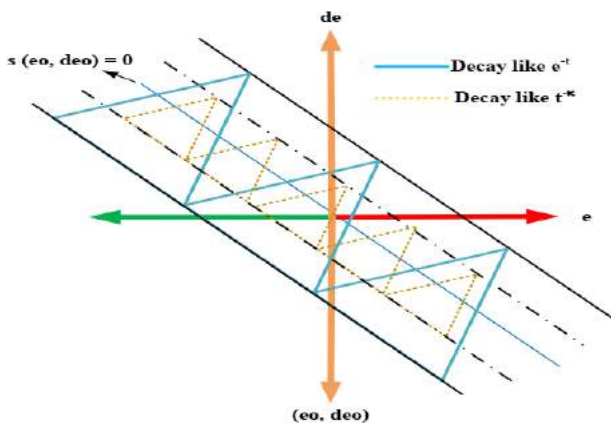


Fig. 5: Stability region of Integer order and Fractional order controller considering same sliding surface for both

Remark 1: *The slow and less intense decay property of fractional order systems can be further exploited for a low value of the total harmonic distortion (THD) of a grid-tied inverter with an L filter.*

2.5 State-Space Representation of PV System

The open-loop system is considered for deriving the state-space formulation of the PV system. By applying Kirchhoff’s voltage and current law, the dynamics of the system are determined. The state-space equations are derived in which the V_{pv} is the PVG output voltage, I_o is inductor current, V_{DC} is the DC-link voltage and I_g is the grid current. Via replacing state-variables V_{pv}, I_o, V_{dc}, I_g by x_1, x_2, x_3, x_4 respectively we attain the following equations:

$$C_{pv} \dot{x}_1 = I_{pv} - x_2 \tag{12.a}$$

$$L_o \dot{x}_2 = x_1 - (1 - \mu_1)x_3 \tag{12.b}$$

$$C_{dc} \dot{x}_3 = (1 - \mu_1)x_2 - \mu_2 x_4 \tag{12.c}$$

$$L_g \dot{x}_4 = \mu_2 x_3 - V_g \tag{12.d}$$

3. Controller Design

As mentioned earlier in the introduction, a back-stepping controller (BSC) is chosen and derived in this section. A conventional BSC is a recursive nonlinear controller that can be used to control dynamic entities in a given model of a system. A FO controller offers more degrees of freedom as compared to the IO controller. In this regard, the slow and intense nature of a FO operator is utilized via FOBSC to reduce oscillations around dynamic entities of the system and enhance the overall power quality. In this section, a modified fractional order operator (D^α) is introduced into conventional BSC; which is presented here as FOBSC that has an extra tuning variable (α) to further intensify the response of derivative and integral of the system dynamics according to our desired response. As shown in Fig. 6, the controller is designed in three different loops. The first loop is designed to track the reference voltage generated by MPPT and regulate the output voltage of PVG to the point where it produces the maximum power. A FOBSC is implemented to achieve a satisfactory tracking of the reference voltage generated by MPPT. The second loop is designed to track a constant voltage reference to keep the voltage of DC-link at the desired level. A fractional-order PI (FOPI) based controller is used for this loop. The third loop is based on FOBSC. In this loop, the output of FOPI is multiplied by grid voltage to generate a sinusoidal reference in phase to the grid. FOBSC is introduced to track this reference and keep the power factor close to unity. Introducing the fractional-order parameter to back-stepping and the PI controller further reduces the THD as compared to conventional methods used till now.

3.1. Fractional-Order PVG Voltage Control

The objective of the first loop is to track the reference voltage (x_1^*) generated by MPPT and regulate the output of PVG ($x_1 = V_{pv}$) close to it. The FOBSC is implemented to track the generated reference. Initially, an error is introduced as:

$$e_1 = C_{pv}(x_1 - x_1^*) \quad (13)$$

where x_1^* is the reference voltage generated by P&O based MPPT. Through the derivative of e_1 and using (12. a), we obtain:

$$\dot{e}_1 = (I_{pv} - x_2 - C_{pv}\dot{x}_1^*) \quad (14)$$

The following Lyapunov stability candidate function is considered to prove stability:

$$V_1 = 0.5e_1^2 \quad (15)$$

Its derivative is given by $\dot{V}_1 = e_1\dot{e}_1$. Choosing $\dot{e}_1 = -c_1e_1$, clearly makes the term $\dot{V}_1 = -c_1e_1^2$ negative definite, as the square will keep the error positive while the negative sign keeps the overall result negative until the term c_1 is positive. Therefore, the system is globally asymptotically stable. Since at this stage, there is no control input therefore, dynamic (that exists in Eq. 14 i.e.) x_2 can be chosen as a virtual control input. Using $\dot{e}_1 = -c_1e_1$ yields:

$$x_2^* = I_{pv} + c_1e_1 - C_{pv}\dot{x}_1^* \quad (16)$$

The new virtual control variable x_2^* is not a real control input, therefore, we require another error. In this error, a new operator has been introduced i.e. D^α which converts the equation to fractional-order. In the above-mentioned operator, D^α, α is further tuned to improve the response of the system.

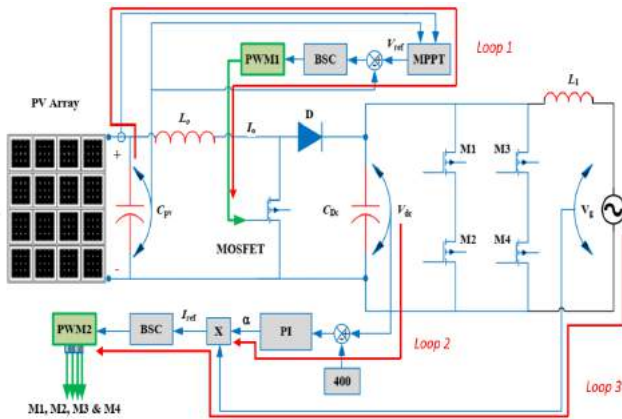


Fig. 6: Block diagram of the system with the considered loops

$$e_2 = L_o D^\alpha(x_2 - x_2^*) \quad (17)$$

The new e_1 and \dot{V}_1 yields as:

$$\dot{e}_1 = -c_1e_1 - \frac{D^{-\alpha}e_2}{L_o} \quad (18)$$

$$\dot{V}_1 = -c_1e_1^2 - D^{-\alpha}e_1e_2/L_o \quad (19)$$

By time derivative of e_2 and using (12. b) we obtain the following equation:

$$\dot{e}_2 = D^\alpha(x_1 - (1 - u_1)x_3 - L_o\dot{x}_2^*) \quad (20)$$

For the stability purposes, the Lyapunov candidate function ($V_2 = 0.5e_2^2 + V_1$) has been chosen. By time derivative of V_2 the equation becomes:

$$\dot{V}_2 = -c_1e_1^2 + e_2\left(\frac{-D^{-\alpha}e_1}{L_o} + \dot{e}_2\right) \quad (21)$$

Choosing $-c_2e_2 = \frac{-D^{-\alpha}e_1}{L_o} + \dot{e}_2$ the above equation becomes negative definite for all positive values of c_2 .

$$\dot{V}_2 = -c_1e_1^2 - c_2e_2^2 \quad (22)$$

Finally, to enforce errors e_1 and e_2 to zero, we simplify the equation to find the control signal as:

$$u_1 = 1 - \frac{1}{x_3}(x_1 + c_2D^{-\alpha}e_2 - L_o\dot{x}_2^* - D^{-2\alpha}e_1/L_o) \quad (23)$$

3.2. Fractional-Order PFC

The same procedure is followed in deriving FOBSC design for power factor control. Since there is only one dynamic at near grid L_g , therefore only one loop is required to control the grid current. The current reference chosen in this case is the multiple of a tuned constant (β) (which is the output of DC-link voltage control) and grid voltage which makes a sinusoidal signal $x_4^* = \beta * V_g$.

The current error is chosen as:

$$e_3 = L_g D^\alpha(x_4 - x_4^*) \quad (24)$$

Time-derivative of e_3 and putting equation (12. d) in \dot{e}_3 we obtain:

$$\dot{e}_3 = D^\alpha(u_2x_3 - V_g - L_g\dot{x}_4^*) \quad (25)$$

Similarly, to find stability a Lyapunov candidate function has been introduced as: $V_3 = 0.5e_3^2$. Using the time derivative yields $\dot{V}_3 = e_3\dot{e}_3$. Choosing $\dot{e}_3 = -c_3e_3$ makes it negative definite.

$$\dot{V}_3 = -c_3e_3^2 \quad (26)$$

To separate the signal of the controller the following equation has been derived:

$$u_2 = \frac{1}{x_3}(V_g + L_g\dot{x}_4^* - c_3D^{-\alpha}e_3) \quad (27)$$

3.3. Fractional Order DC-link Voltage Control

One of the main challenges of PVG based inverter is the voltage across the DC-link capacitor. The power delivered by the PVG is fed to the DC-link capacitor while inverter draws the same power from it, while, at the same time a number of fluctuations are experienced by this element. At the time the PVG generate power, the capacitor voltage rises due to an

increase in input power. Similarly, when inverter draws power from it, consequently voltage decreases across the DC-link capacitor. Due to significant increasing and decreasing phenomena of DC-link voltage, the output of the inverter is distorted thereby the grid power quality will be reduced. To tackle this issue, a control loop is required to keep the DC-link voltage constant. A DC-link voltage level should be greater than the grid voltage as explained in [14]. A Fractional proportional-integral (PI) based controller is applied to regulate the voltage across DC-link. The output of the PI regulator acts as a current reference (β) which is further multiplied by grid voltage to generate a sinusoidal current reference.

$$\beta = (K_p + K_i D^{-\alpha})(x_3^2 - x_3^{*2}) \quad (28)$$

Where K_p is the proportional gain, K_i is the integral gain and the DC-link voltage is squared to make the response of the regulator faster.

4. Results and Discussions

To verify the practicality of the proposed controller, a PVG having the maximum capacity of 1492W is tested in MATLAB/SIMULINK. The system specifications are given in Table 1. The IO controller is implemented according to [12]. The whole system is tested for FO controller as well as IO controller. To check the system performance three case-scenarios are studied. In the first case, the time-steps are considered from 0 to 0.5 seconds. Steady-state performance is evaluated by using ideal input parameters for PVG as 1000 W/m^2 Irradiance and 25°C Temperature. As it can be seen from Fig. 7a and 7b, the power output of PVG in this case is almost 100% (1492W) which is considered to be an ideal condition. In the second test case, the time-steps are considered to vary from 0.5 to 0.8 seconds. The system is evaluated for 80% of PVG capacity which is equal to 1202W. The irradiance and temperature inputs are 800 W/m^2 and 30°C , respectively. In the third case, the capacity of PVG is kept at 70% of the rated power which is equal to 1050.5 W. 700 W/m^2 irradiance and 35°C are chosen in this case where the time-steps varies from 0.8 to 1seconds.

In Fig. 8 to 11, the study has investigated the DC side performance of the system. Figures 10 and 11 show the boost inductor current and PV output capacitor voltage. In case 1, the response of the system has been tested in an ideal weather condition. The steady state response clearly show that the FO controller has outperformed the IO controller. The current in FO controller resides around 7.3 A with smaller oscillations between the highest and the lowest peak. This shows that the charging and discharging phenomena of boost inductor has been improved. This effect has clearly reduced the width of the ripple. The advantage of slow and intense nature of the FO controller has also been seen in the output voltage of PV in Fig. 11. It is evident from the PVG IV-curve that maximum output power is drawn at 203V output. The voltage in Fig. 11 in FO controller is almost

203V with least oscillations between maximum charging and discharging points of PV output capacitor.

As voltage and current both have been improved, the power output in Fig. 9 is also enhanced not only in terms of oscillations but also in capacity. The power output via FO controller is above 1490.5W which is close to the ideal capacity of PVG i.e. 1492W while in IO controller the power capacity is seen to be oscillating around 1487W. Effect of FO controller is observed in P&O output reference voltage in Fig. 8. Similarly, in case 2 and 3, the reference generation in terms of FO controller compared to IO is much closer to the I-V curve. FO controller offers a reduction in peaky oscillations thereby the average power is also increased. In all the three cases, the FO controller has shown least oscillations in power while a higher average power generation capacity (considering the graph of FO controller is slightly above the IO controller graph). Additionally, the dynamic behavior of the system in case 2 and 3 is far better using FO controller as observed in Fig. 9. The lowest peak in case 2 and 3 is approximately appeared at 1158W at 0.5 sec and 975W at 0.8 sec for IO controller, where in case of FO controller it occurs at 1169W at 0.5 sec and 985 W at 0.8 sec.

Table 1: Specifications of the complete system

No.	Parameters	Values
1	Module Type: Soltech 1STH-215-P	1
2	Parallel strings	1
3	Series panels	7
4	PV Open-circuit voltage, V_{oc}	36.4 V
5	PV Short-circuit current, I_{sc}	7.84 A
6	PV maximum power point voltage, V_{mpp}	29 V
7	PV single panel maximum output power	215 W
8	PV total output power capability	1492 W
9	PV output capacitor, C_{pv}	0.2 mF
10	Boost converter Inductor, L_o	100 mH
11	DC-link capacitor, C_{dc}	5 mF
12	BSC controller constant, c_1	500,000
13	BSC controller constant, c_2	500
14	PWM boost converter, S_1	100 KHz
15	FOBSC tuning order, α_2	0.6
16	Grid filter inductor, L_g	9 mH
17	BSC controller constant, c_4	500,000
18	PWM inverter, S_2	10 KHz
19	FOPI tuning order, α	0.95
20	FOBSC tuning order, α_1	0.875

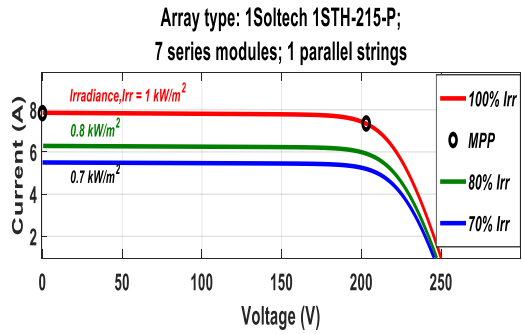


Fig. 7a: Effect of Irradiance on solar PV output

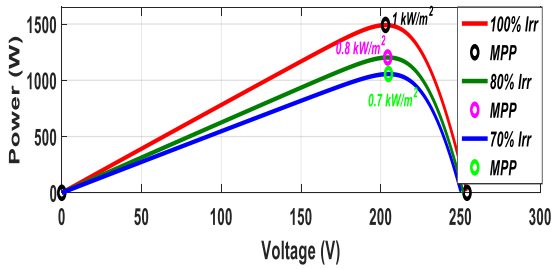


Fig. 7b: Effect of temperature on solar PV output

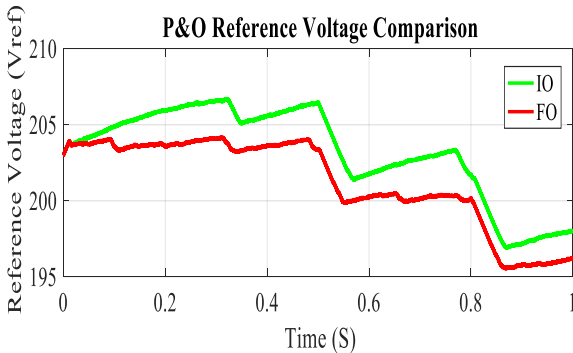
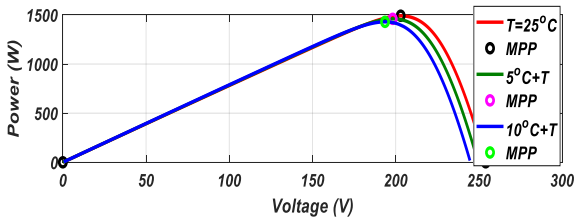
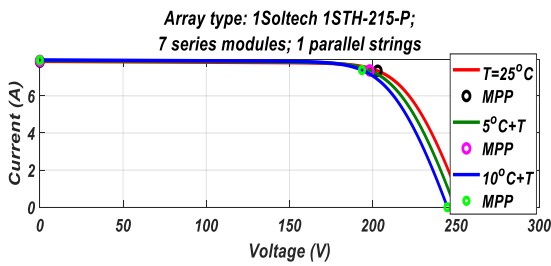


Fig. 8: P&O Reference Voltage – V_{ref}

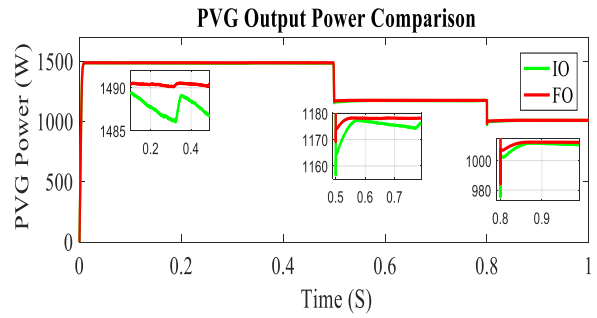


Fig. 9: Maximum Output Power of PVG

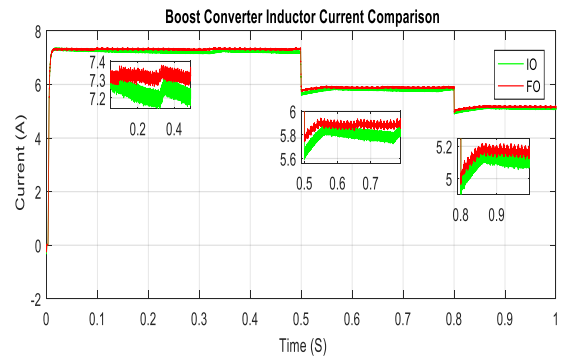


Fig. 10: Boost Converter Inductor Current

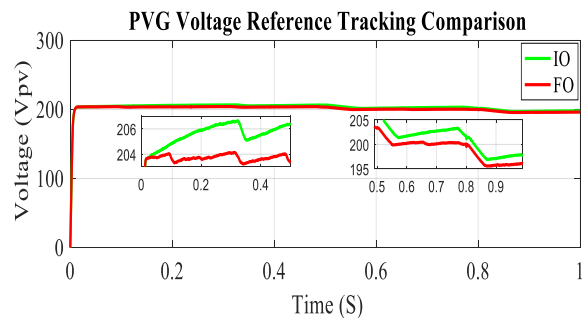


Fig. 11: PVG Voltage

Figures 12 to 15 show response of the AC part of the system, representing; grid current, real power, reactive power and power factor of grid respectively. Fig. 12 shows the grid current in terms of FO and IO, being compared to the reference current generation of the grid. As discussed earlier, the slow and intense nature of the FO controller offers a more fluctuation-free real power of 1405 W and reactive power of -54 VAR in case 1 of Fig. 13 and 14. The output power of the PV in terms of FO was found to be 1490.5 W. The power losses in this case for boost converter and inverter are about 5.736%. In case 2, the real and reactive power is around 1093W and -42.5VAR. Real and reactive powers in case 3 are observed to be 925W and -36VAR. In all the three cases, the real powers of the IO controller are 1399W, 1088W and 921W while reactive powers are -53VAR, -41.5VAR and -34VAR, respectively. The steady state power losses in the IO controller is approximately 5.917%. Due to less intense nature of FO controller, reduction of oscillation occurs, therefore, the power factor in Fig. 15 is also witnessed to be increased. During case 1, the power factor is nearly 0.9985 for FO controller and 0.998 for IO controller.

In case 2 and 3, the PF in IO controller is significantly lower i.e. 0.9973 while FO controller still offers a higher PF of 0.9984.

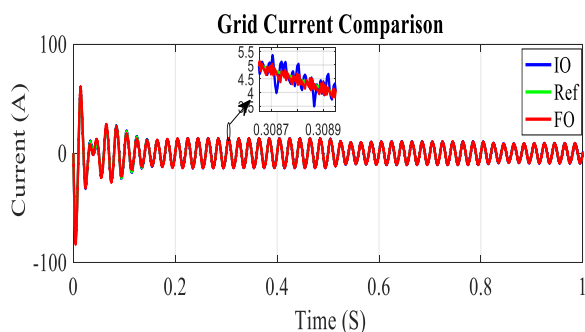


Fig. 12: Comparison of the grid current

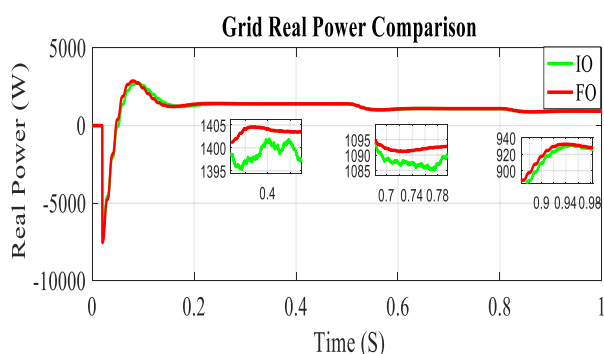


Fig. 13: Real Power Comparison

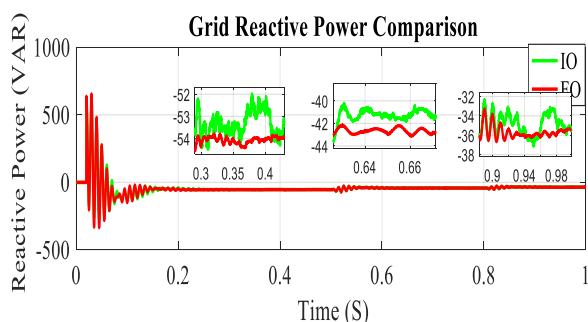


Fig. 14: Reactive Power Comparison

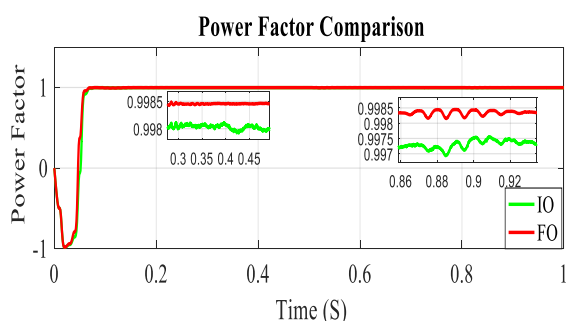


Fig. 15: Power Factor Comparison

The comparison of all the obtained THDs is presented in Table 2. According to the results, the FO controller has achieved considerably lower THDs in comparison to IO controller. FO controller offers THD of 4.04%, 4.19% and 4.56% for three studied cases where for the same cases IO offers 4.99%, 5.62% and 6.42%, respectively.

Table II: Specifications of the complete system

Cases	FO Controller	IO Controller
Case 1	4.05%	5%
Case 2	4.19%	5.62%
Case 3	4.56%	6.42%

System efficiency is given in Fig. 16. As the FO controller offers smooth response in terms of oscillation thereby reducing the power losses compared to the IO controller. Therefore, the overall effect is felt on the efficiency of the overall system.

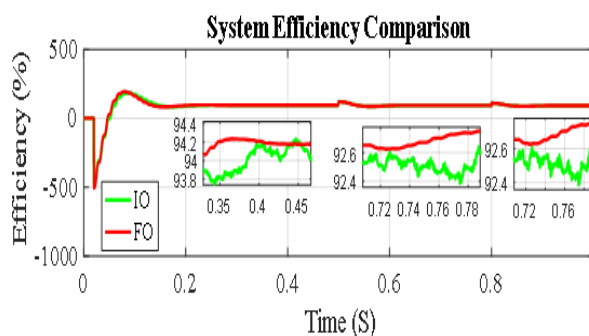


Fig. 16: System Efficiency

5. Conclusion

A non-Linear FOBS system is developed in this study. The functionality of the proposed system is tested in MATLAB/SIMULINK. The findings of this study can be precisely presented as follows:

- The results have verified that the slow and intense nature of the FO controller can be used to enhance the power-quality of the system.
- The output power of the PVG in case of FO controller contains less oscillations than IO controller, hence the reduction of power losses is observed, which consequently improves the power generation capacity of the PVG.
- Results have shown that the FO controller develops voltages and currents with reduced oscillations in waves across the systems dynamics such as PV capacitor, boost and grid inductor.
- It is well observed in the given results that sine wave of FOBS controller is superior over the IO controller. In the conventional method, the IO controller THD is calculated as 4.99% in case 1 while in the proposed method has reduced the THD to 4.05%. According to IEEE standards, THD should be less than 5%. In two other cases, the THD of IO controller crosses the IEEE limit while the proposed controller still maintains IEEE standard.
- The proposed controller also outperforms the

conventional controller in terms of power loss. A total of 5.736% of system power losses are calculated under FO controller while in IO the system experiences about 5.917% losses.

- The power factor of the inverter is very close to unity in both controllers whereas the proposed controller offers a higher power factor compared to the IO controller. During the steady state condition, the FO controller offers the PF around 0.9985 while in IO is slightly low i.e. 0.998. During reduction in available irradiance and change in temperature, the FO offers PF of 0.9984 while the IO shows PF of about 0.9974.

Acknowledgment

This work has been partially supported by the Post-doctoral International Exchange Fellowship Program 2018 (Talent-Introduction Program 2018) of the P. R. China (Fund No. 207689).

References

- [1] S. Mishra, D. Pullaguram, S. AcharyBuragappu and D. Ramasubramanian, "Single-phase synchronverter for a grid-connected roof top photovoltaic system", *IET Renewable Power Generation*, Vol. 10, pp. 1187-1194, 2016.
- [2] N. Dai, M. Wong, J. Guerrero and et al, "Analysis, control and experimental verification of a single-phase capacitive-coupling grid-connected inverter", *IET Power Electronics*, Vol 8, pp. 770-782, 2015.
- [3] S. S, K. Chatterjee and S. Bandyopadhyay, "One-Cycle-Controlled Single-Stage Single-Phase Voltage-Sensorless Grid-Connected PV System", *IEEE Transactions on Industrial Electronics*, Vol. 60, pp. 1216-1224, 2013.
- [4] M. Islam, S. Mekhilef and M. Hasan, "Single phase transformerless inverter topologies for grid-tied photovoltaic system: A review", *Renewable and Sustainable Energy Reviews*, Vol. 45, pp. 69-86, 2015.
- [5] M. Al Ahmad and K. Islam, "Combined Constant Voltage and Perturb and Observe Method Based Algorithm for Fast and Efficient Maximum Power Point Tracking Using Buck-Boost Converter", *Journal of Green University of Bangladesh*, vol. 4, pp. 36-43, 2013.
- [6] I. Kirpichnikova and A. A. Maliugina, "The energy efficiency of photovoltaic power plants", *2nd International Conference on Industrial Engineering, Applications and Manufacturing (ICIEAM)*, pp.1-3, Chelyabinsk 2016.
- [7] M. Carlos, B. Domingo, M. Juan and G. Francesc, "Boost-buck inverter variable structure control for grid-connected photovoltaic systems with sensorless MPPT", *Proceedings of the IEEE International Symposium on Industrial Electronics (ISIE)*, vol. 2, pp. 657-662, 2005.
- [8] M. Lasheen, A. Abdel Rahman, M. Abdel-Salam and S. Ookawara, "Adaptive reference voltage-based MPPT technique for PV applications", *IET Renewable Power Generation*, Vol. 11, pp. 715-722, 2017.
- [9] M. de Brito, L. Galotto, L. Sampaio and et al., "Evaluation of the Main MPPT Techniques for Photovoltaic Applications", *IEEE Transactions on Industrial Electronics*, Vol. 60, pp. 1156-1167, 2013.
- [10] V. Lal and S. Singh, "Control and Performance Analysis of a Single-Stage Utility-Scale Grid-Connected PV System", *IEEE Systems Journal*, Vol. 11, pp. 1601-1611, 2017.
- [11] N. Zakzouk, A. Abdelsalam, A. Helal and B. Williams, "PV Single-Phase Grid-Connected Converter: DC-link Voltage Sensorless Prospective", *IEEE Journal of Emerging and Selected Topics in Power Electronics*, Vol. 5, pp. 526-546, 2017.
- [12] C. Aouadi, A. Abouloifa and I. Lachkar and et al., "Nonlinear Controller Design and Stability Analysis for Single-Phase Grid-Connected Photovoltaic Systems", *International Review of Automatic Control (IREACO)*, Vol. 10, no. 4, pp. 306, 2017.
- [13] A. Martin, J. Cano, J. Silva and J. Vazquez, "Backstepping Control of Smart Grid-Connected Distributed Photovoltaic Power Supplies for Telecom Equipment", *IEEE Transactions on Energy Conversion*, Vol. 30, pp. 1496-1504, 2015.
- [14] M. Boztepe, F. Guinjoan, G. Velasco-Quesada and et al, "Global MPPT Scheme for Photovoltaic String Inverters Based on Restricted Voltage Window Search Algorithm", *IEEE Transactions on Industrial Electronics*, Vol. 61, pp. 3302-3312, 2014.
- [15] M. Aghababa, "A Lyapunov-based control scheme for robust stabilization of fractional chaotic systems", *Nonlinear Dynamics*, Vol. 78, pp. 2129-2140, 2014.
- [16] F. Zhang and C. Li, "Stability Analysis of Fractional Differential Systems with Order Lying in (1, 2)", *Advances in Difference Equations*, pp. 1-17, 2011.
- [17] Z. Gao and X. Liao, "Improved Oustaloup approximation of fractional-order operators using adaptive chaotic particle swarm optimization", *Journal of Systems Engineering and Electronics*, Vol. 23, n. 1, pp. 145-153, 2012.
- [18] B. T. Zhang, P. I. YG and Y. Luo, "Fractional order sliding-mode control based on parameters auto-tuning for velocity control of permanent magnet synchronous motor", *ISA Transactions*, Vol. 51, no. 5, pp. 649-656, 2012.
- [19] N. Ullah, S. Wang, K. Muhammad Irfan, S. Muhammad, "Fractional order adaptive fuzzy sliding mode controller for a position servo system subjected to aerodynamic loading and nonlinearities", *Aerospace Science and Technology*, Vol. 43, pp. 381-387, 2015.
- [20] N. Ullah, H. Songshan, K. Muhammad Irfan, "Adaptive fuzzy fractional-order sliding mode controller for a class of dynamical systems with uncertainty", *Transaction of Institute of Measurement and Control*, Vol. 38, pp. 402-413, 2015.

- [21] S. Nouredine and A. Ahmed, "Nonlinear control for MPPT and UPF of PV system connected to the grid", *7th International Renewable Energy Congress (IREC)*, pp. 1-6, 2016.
- [22] J. Muhammad Yaqoob, L. Qiang, R. Hassan, S. Yasir and G. Muhammad Majid, "Design and implementation of a single-phase multilevel cascaded inverter for PV system", *International Conference on Smart Grid and Clean Energy Technologies (ICSGCE)*, pp. 201-206, 2016.
- [23] H. Manel, G. Gabriele and R. Massimo, "An improved MPPT algorithm based on hybrid RCC scheme for single-phase PV systems", *IECON 2016 - 42nd Annual Conference of the IEEE Industrial Electronics Society*, pp. 3024-3029, 2016.
- [24] A. EL Faicel, M. Hattab, M. Azeddine, H. Muhammed, "A new strategy to control the active and reactive power for single phase grid-connected PV inverter", *3rd International Renewable and Sustainable Energy Conference (IRSEC)*, pp. 1-6, 2015.
- [25] L. Guihua, Y. Yulin, W. Pangbao, W. Wei and D. Xu, "Stability control method based on virtual inductance of grid-connected PV inverter under weak grid", *IECON 2013 - 39th Annual Conference of the IEEE Industrial Electronics Society*, pp. 1867-1872, 2013.
- [26] S. Rajendran and D. Jena, "Backstepping sliding mode control of a variable speed wind turbine for power optimization", *Journal of Modern Power Systems and Clean Energy*, Vol. 3, pp. 402-410, 2015.
- [27] S. Fahad, A. J. Mahdi, W. H. Tang, K. Huang and Y. Liu, "Particle Swarm Optimization Based DC-link Voltage Control for Two Stage Grid Connected PV Inverter", *2018 International Conference on Power System Technology (POWERCON)*, pp. 1-9, 2018.
- [28] Y. Mahmoud and E. El-Saadany, "Accuracy Improvement of the Ideal PV Model," in *IEEE Transactions on Sustainable Energy*, vol. 6, no. 3, pp. 909-911, July 2015.
- [29] H. Cha and T. Vu, "Comparative analysis of low-pass output filter for single-phase grid-connected Photovoltaic inverter," *2010 Twenty-Fifth Annual IEEE Applied Power Electronics Conference and Exposition (APEC)*, Palm Springs, CA, 2010, pp. 1659-1665.
- [30] P.Nammalvar, S.Ramkumar and R.Umadevi, "Cost Effective Solitary Stage Single Phase Inverter for Solar PV Integration in to Grid", *International Journal of Renewable Energy Research*, Vol.8, No.3, pp. 1309-1317.
- [31] F. Xiao, L. Dong and X. Liao, "A single-phase grid-connected PV inverter with improved grid-connected current," *The 27th Chinese Control and Decision Conference (2015 CCDC)*, Qingdao, 2015, pp. 4083-4088.
- [32] A. M. Mnider, D. J. Atkinson, M. Dahidah and M. Armstrong, "A simplified DQ controller for single-phase grid-connected PV inverters", *2016 7th International Renewable Energy Congress (IREC)*, Hammamet, 2016, pp. 1-6.
- [33] H. El Fadil and F. Giri, "MPPT and Unity Power Factor Achievement in Grid-Connected PV System Using Nonlinear control", *IFAC Proceedings Volumes*, Vol. 45, Issue 21, pp. 363-368, 2012.
- [34] M. Aourir, A. Abouloifa, I. Lachkar, A. Hamdoun, F. Giri, F. Cuny, "Nonlinear Control of PV System Connected to Single Phase Grid through Half Bridge Power Inverter", *IFAC-PapersOnLine*, Vol. 50, Issue 1, pp. 741-746, 2017.
- [35] L. Ammeh, H. El Fadil, A. Yahya, K. Ouhaddach, F. Giri, T. Ahmed-Ali, "A Nonlinear Backstepping Controller for Inverters used in Microgrids", *IFAC-PapersOnLine*, Vol. 50, Issue 1, pp 7032-7037, 2017.
- [36] G. R. Chandra Mouli, J. H. Schijffelen, P. Bauer and M. Zeman, "Design and Comparison of a 10-kW Interleaved Boost Converter for PV Application Using Si and SiC Devices," in *IEEE Journal of Emerging and Selected Topics in Power Electronics*, vol. 5, no. 2, pp. 610-623, June 2017.
- [37] S. Dutta and K. Chatterjee, "A Buck and Boost Based Grid Connected PV Inverter Maximizing Power Yield From Two PV Arrays in Mismatched Environmental Conditions," in *IEEE Transactions on Industrial Electronics*, vol. 65, no. 7, pp. 5561-5571, July 2018.
- [38] R. S. Muñoz-Aguilar, I. Candela, J. Rocabert and P. Rodríguez, "Grid resonance attenuation in long lines by using renewable energy sources," *2017 IEEE 6th International Conference on Renewable Energy Research and Applications (ICRERA)*, San Diego, CA, 2017, pp. 429-434.
- [39] D. M. Ionel, "Keynote speakers: Plans for 100% renewable energy and requirements for technological developments," *2016 IEEE International Conference on Renewable Energy Research and Applications (ICRERA)*, Birmingham, 2016, pp. 11-15.
- [40] S. S. Dash, "Tutorial 1: Opportunities and challenges of integrating renewable energy sources in smart," *2017 IEEE 6th International Conference on Renewable Energy Research and Applications (ICRERA)*, San Diego, CA, 2017, pp. 19-23.
- [41] D. P. Andrea, D. N. L. Pio and M. Santolo, "Super twisting sliding mode control of smart-inverters grid-connected for PV applications," *2017 IEEE 6th International Conference on Renewable Energy Research and Applications (ICRERA)*, San Diego, CA, 2017, pp. 793-796.
- [42] M. Quraan, Q. Farhat and M. Bornat, "A new control scheme of back-to-back converter for wind energy technology," *2017 IEEE 6th International Conference on Renewable Energy Research and Applications (ICRERA)*, San Diego, CA, 2017, pp. 354-358.